

Measuring Perfusion Using Magnetic Resonance Imaging

Paula Myers, pdmyers@xula.edu

Advisor: Dr. H. Michael Gach, University of Pittsburgh Department of Radiology and Bioengineering, gach+@pitt.edu

Abstract

Perfusion Magnetic Resonance Imaging (MRI) measures the rate at which blood is delivered to tissue. The measure of perfusion acts as an indicator of tissue health. Applications of perfusion imaging include the diagnosis of both acute and chronic disease and the study of micro vascular changes associated with functional cerebral activation. An influential advantage of MRI is that it has no ionization radiation as in x-ray techniques. Further development of techniques in MRI enables us with new ways to study the brain in great detail. Arterial spin labeling (ASL) is a noninvasive perfusion MRI technique that uses radio frequency (RF) to invert the arterial spins (magnetization). A control image (spins not inverted) is also obtained. The perfusion is proportional to the difference (control -label) image. Analyzing the perfusion kinetics requires the evaluation of several hemodynamic and MRI variables. The arterial velocity term will be the main focus of this experimental evaluation. Blood flow was simulated using a water mixture that has the same MR properties as blood. The velocity was measured by using phase contrast MRI imaging the fluid as it flowed through a pulsatile flow phantom. In addition, T1 and B1 were measured with MRI using saturation recovery and variable nutation techniques, respectively.

I. Introduction

Magnetic resonance imaging (MRI) ^{1-a} is an imaging technique used primarily in medical settings to produce high quality images of the inside of the human body. Felix Bloch and Edward Purcell discovered this technique in 1946 ^{1-a}. Both were awarded the Nobel Prize in 1952 for the discovery. Between 1950 and 1970 Nuclear Magnetic Resonance (NMR) ^{1-a} was developed for molecular and chemical analysis. In September

of 1971 Paul Lauterbur ^{1-b} of the State University of New York at Stony Brook applied magnetic field gradients in all three dimensions and used the back-projection technique to create the first NMR images. With this new technique, zeugmatography, Lauterbur opened the field to imaging. In 1975 Peter Mansfield ^{1-b} along with Andrew A. Maudsley proposed a line scan technique. This technique in turn led to the first in vivo image of the human anatomy in 1977. By 1978, Peter Mansfield presented the first image through the abdomen. Also in 1971 Raymond Damadian ² showed that the nuclear magnetic relaxation times differed for tissues and tumors. This discovery gave way to this technique being used to detect disease. In 1975 Richard Ernst ³ introduced magnetic resonance imaging using phase and frequency encoding and the Fourier Transform, all of which are the basis of most existing MRI principles. By 1986 the typical imaging time was reduced from five minutes to five seconds. The technique was called magnetic resonance imaging rather than nuclear magnetic resonance imaging (NMRI) because of the negative connotations associated with the word nuclear in the late 1970's ¹. MRI has advanced beyond a tomographic imaging technique to a volume imaging technique. MRI provides an unparalleled view of the human body by producing 2D images or 3D models. The uses of MRI for diagnostic purposes vary from diagnosing multiple sclerosis, brain infections and tumors, to visualizing torn ligaments and shoulder injuries.

As with any technique there are also advantages and disadvantages to using MR imaging ⁴. There are very low incidences of side effects. MR imaging requires no ionizing radiation and as images are given in any plane, repositioning of the patient is not required. An MRI system can create axial images as well as images in the sagittal plane (slicing the bread side-to-side lengthwise) and coronally or any degree in between as shown in Figure 3. On the down side, pacemakers cannot be placed in the magnet. Also screws, plates, and artificial joints cause artifact in scanned images. Aside from being expensive, there are also other limitations such as weight, elevated noise levels, and claustrophobic conditions to name a few.

Perfusion MRI ⁵ is one of the rapidly developing areas of imaging application. Perfusion ⁵ describes the amount of blood delivered to the capillary beds of a block of tissue in a certain time period. This quantity determines whether the tissue is in any

grave danger. These applications include the study of blood flow in an effort to diagnose disease in areas such as the brain. This is possible partly because perfusion measurements reflect the delivery of essential nutrients to specific tissue. In measuring perfusion there are specific terms that must be evaluated and certain methods by which these terms are evaluated and the data reviewed. The aim of this report is to describe the methods by which the perfusion value (difference control-label) is evaluated through several related terms including T1, the spin lattice relaxation constant, velocimetry, and B1, the radiofrequency magnetic induction field, and to understand the data obtained by this evaluation. This will be explained according to the following format:

- I. Introduction
- II. Theory
- III. Experimental Setup
- IV. Results
- V. Discussion and Conclusion
- Acknowledgements
- References

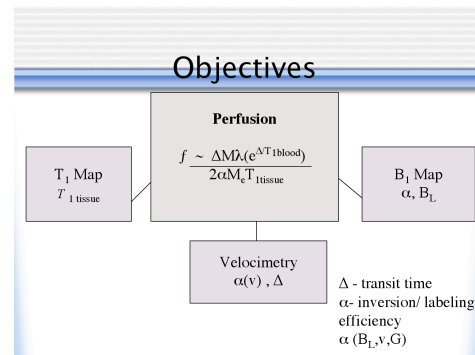


Figure 1:
Main points of outline goals

II. Theory

The perfusion is given by the equation:

$$f \sim \frac{[\Delta M] e^{\Delta/T1^{blood}}}{2\alpha M_e T1^{tissue}}$$

and is proportional to the difference (label-control) signal (ΔM). In order to evaluate this equation several quantities must be evaluated as diagramed in Fig.1. These required quantities include T1, velocity, and B1. We will address how we measure these three parameters herein. Other quantities in this equation include α which is the blood partition coefficient typically assumed to be 0.9. The arterial transit time Δ is defined as the time required to travel from the labeling plane to the tissue. M_e is the equilibrium magnetization and α is the inversion/labeling efficiency.

$T1^6$ is the spin lattice time constant for magnetization to return to equilibrium. This parameter is estimated with least squares fitting using two or three parameter nonlinear models.

Velocimetry measures the speed and direction of the evaluated flow using Phase Contrast Cine to give the velocity at multiple time points. The velocimetry relates to the perfusion equation because it is needed to determine the term λ , the inversion/labeling efficiency. The equations relating λ to the velocity and $B1$ are as follows:

$$\lambda = 1 - e^{-\lambda^2/2};$$

$$\lambda = \lambda B_1^2 / G \cdot V;$$

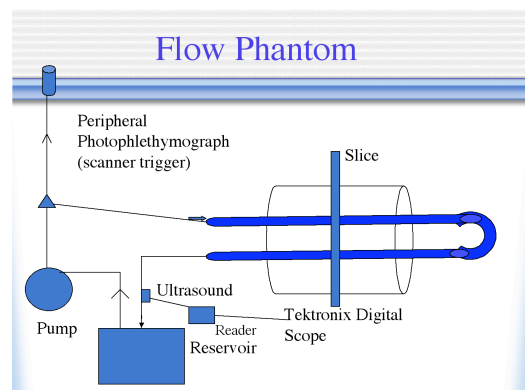
$$\lambda = 2 \lambda * 4257 (\text{Hz/gauss}) - (\text{gyro magnetic ratio for 'H (protons)})$$

$B1^7$ is the radiofrequency magnetic induction field. This term is considered to be composed of two oppositely rotating vectors, but the $B1$ we use in our quadrature coils is polarized so that there are not two oppositely rotating vectors. The $B1$ magnetic field is important because in MRI this radio frequency field excites the nuclei⁸ and nutates (rotates) their magnetic moment, normally aligned along the longitudinal z-axis of the static magnetic field ($B0$), down into the transverse x-y plane.

III. Experimental Setup

To obtain measurements, the following equipment was used: GE 1.5T Signa LX MRI whole body scanner, flow simulation equipment (flow phantom) powered by a Harvard pulsatile pump, a Transonic Systems Doppler Ultrasound, and a Tektronix digital oscilloscope (fig. 2). Flow was simulated through the phantom by

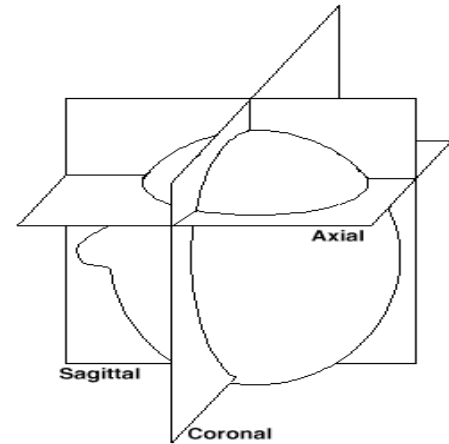
Figure 2: Phantom setup



water pumped by the pulsatile pump. As the fluid continuously flows, the phantom is scanned in the MRI scanner. The scanner images the phantom in one slice as shown in Fig. 3 (Note: One can acquire more slices but it takes more time). This slice is axial and

is perpendicular to the direction of flow. This data is then collected for a period of processing and evaluation. It is this process that yields the necessary components for evaluation.

Figure 3:
Example of slices as imaged using MRI



IV. Methods

1. T1 Maps

Phantom Measurements

T1 is measured using a saturation recovery pulse sequence in which the magnetization is nutated (rotated) into the transverse plane and then imaged after a variable recovery delay. As the delay is increased, the amount of image signal (representing the relaxed magnetization) increases. To obtain the T1 information for the phantom, raw k-space data was acquired from the scanner and then reconstructed into images. The mean signal intensities of the entire image were then taken for twelve repetitions. The repetitions were plotted as mean intensity signals vs. recovery delay time. The acquisition timings were sampled in such a way that the mean intensities were exponentially distributed for the repetitions. The intensities were then fitted using a three-parameter model: $y = A + Be^{cx}$ to acquire the value C.

2. PC Cine Velocimetry

Flow velocity was measured using a Phase Contrast Cine pulse sequence in which the flow velocity is encoded into the phase of the magnetization. The pulse sequence is designed to produce a signal phase that is directly proportional to the flow velocity. This technique is based on the principle that moving magnetic moments (or spins) acquire a phase in the presence of a magnetic field gradient. The phase is determined from the arctangent of the real and imaginary components of the MR signal (since the signals are received using a quadrature receiver). Velocimetry data for the phantom measurements was acquired from both a Transonic Doppler ultrasonic flow probe and the phase contrast cine maps provided by the scanner. The data was then analyzed using Excel. The data extracted from the ultrasound probe was time vs. voltage. The voltage was then converted

to velocity (cm/s) using a conversion factor of 46.95 cm/(s*volt). The velocity was then graphed as a function of time and scaled to coincide with the flow measurements provided by the phase contrast cine maps which were obtained by recording the mean (mm/s) quantity displayed on the scanner. From the PC Cine maps, data from two regions of interest (ROI) per slice was recorded. ROI 1 represented forward flow and ROI 2 represented return flow. The data was also graphed in Excel as velocity vs. time. The time value was expressed by multiplying the period by each image number. (Ex. Slice n: $(n/20)*T$). The two data sets were then graphed together time synchronized and scaled to coincide.

3. B1 Map

B1 was measured for a human sample using a variable nutation pulse sequence in which the amplitude of the flip angle was incrementally varied from 0° to 180°. The resulting signal curve was used to determine the pixel by pixel distribution of B1 between and within each image plane (or slice). This data represented the signal intensities for twenty repetitions pixel by pixel. To obtain the B1 information a raw k-space data file (or P- file) was extracted from the scanner. Each P-file consists of twenty repetitions with each repetition containing nineteen slices. Each P-file was then reconstructed to get an image file. From the image file a small region of interest (roi) was chosen. From these regions twenty signal intensities were acquired. These signals were averages of all the intensities within the chosen region of interest. B1 was also obtained using curve fitting. Here the three-parameter model $A + B \sin(c x)$ was used where x represents the input flip angle.

These reconstructed images were also motion corrected. High-resolution images were acquired for spatial information. These two sets of images were then co-registered. The high-resolution images underwent a process of segmentation that divided them into three separate parts: gray matter, white matter, and cerebral spinal fluid (CSF). The high-resolution segmented images were then resliced along with the corresponding low-resolution images to get low-resolution segmented images. From the low-resolution images, an average of T1 for the corresponding gray and white matter tissues was obtained. With these low-resolution segmented images, the tissue regions in the motion corrected images were located. For these tissue regions T1 within was acquired on a pixel

by pixel basis and averaged for gray and white matter. The T1 within for each pixel was obtained after fitting the intensities for the twelve time samples. The TR (repeat time) of the sample was 8 s and the T1 of the sample was 1 s.

V. Results

T1 Map

The data in Figure 4 shows the results of a nonlinear fit that was applied to the data in Table 1. The recovery curve represents magnetization returning to its equilibrium value. By fitting this data, the variable C is obtained. C is equal to $1/T_1$. T1 is one of the required variables for the general perfusion (difference control-label) equation. The constant values are given as $A= 70,000$; $B= -40,000$; c the term of interest was assumed to be 1.

Table 1: T1 data

Mean signal	Time (s)
21608.3535	0
22786.3105	0.085
24784.3066	0.17
26915.6699	0.255
28815.2676	0.34
32329.7227	0.51
35621.8086	0.68
39018.6211	0.85
46280.4922	1.275
52496.7539	1.7
57792.9688	2.125
62493.1094	2.55

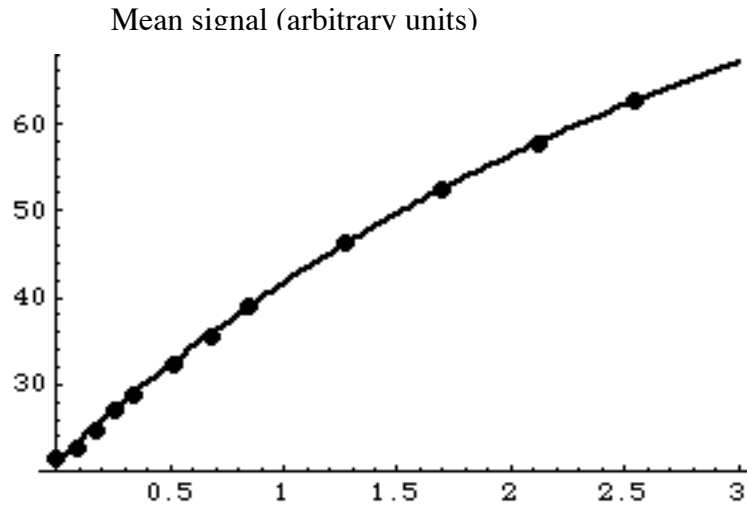


Figure 4: Fitted T1 saturation curve for water phantom: 0.25 mM $\text{CuSO}_4 \cdot 5\text{H}_2\text{O}$; 30 mM NaCl. Measured at 3T in phantom
X-axis: recovery delay, Y-axis: signal representing magnetization.

The T1 value for Figure 4 was found to be 3.014. The estimated error in T1 was 0.1465.

Velocimetry

The velocimetry data is given in two forms. The first form is shown in Fig. 5. This is the data from the ultrasound and the phase contrast cine maps before scaling. The latter demonstrates scaling in an effort to coincide the two data sets. The data was scaled using an equation $A*y$, where y was the value of the regions of interest (ROI 1, ROI 2) and A was the scale factor. The scale factors were 1.2 and 1.12 for ROI 1 and ROI 2, respectively. The chi square for (ROI 1), calculated as an average squares deviation, in the scaled figure (Fig. 6) was estimated to be 15.68. The uncertainty in the same figure for (ROI 2) was estimated as 9.021.

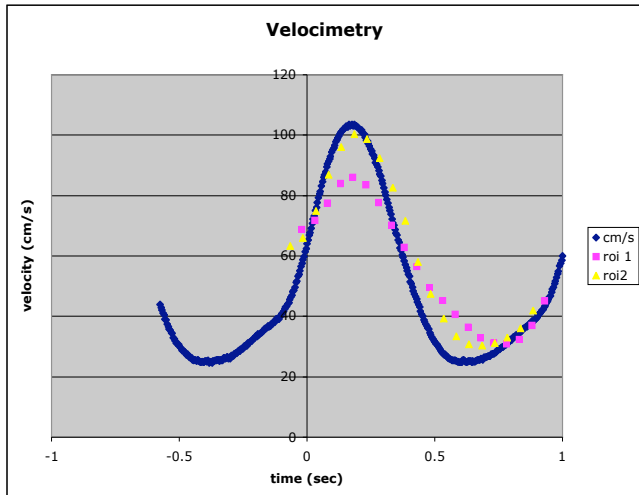
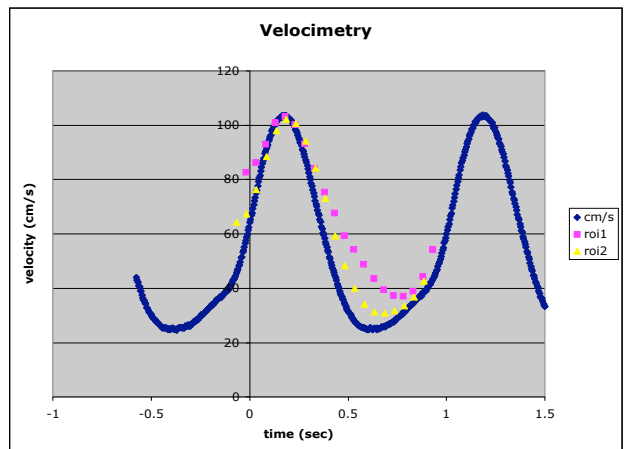


Figure 5:
Un scaled velocimetry data X-axis: time, Y-axis: flow rate

Table 3: mean volume flow rates

Ultrasound	ROI 1	ROI2
50.63(cm/s)	53.04(cm/s)	51.41(cm/s)

Figure 6: Scaled velocimetry data
X-axis: time, Y-axis: flow rate



B1 Map: The B1 curves were obtained by fitting the data shown in Table 2. By fitting this data the value of the variable C was obtained. This variable is then used in the equation: $B1=0.146 \cdot C$ gauss. The flip angle is then calculated using the equation: $\alpha = C \cdot 180^\circ / \pi$.

Table 2: B1 mapping data sets one and two

Data Set 1 Intensity	Input Flip angle (Radians)	Data Set 2 Intensity	Input Flip angle (Radians)
0.7723	0.2	0.7990	0.2
1.0728	0.3	1.1205	0.3
1.3036	0.4	1.4270	0.4
1.5960	0.5	1.6897	0.5
1.7621	0.6	1.9086	0.6
1.9253	0.7	2.0990	0.7
2.0021	0.8	2.2237	0.8
2.0970	0.9	2.3085	0.9
2.0888	1.0	2.3632	1.0
2.0880	1.1	2.2924	1.1
2.0361	1.2	2.2699	1.2
1.9453	1.3	2.1921	1.3
1.8265	1.4	2.0225	1.4
1.7149	1.5	1.8798	1.5
1.5211	1.6	1.6872	1.6
1.3569	1.7	1.5258	1.7
1.1795	1.8	1.3163	1.8
1.0233	1.9	1.1184	1.9
0.9151	2.0	0.9083	2.0
0.7878	2.1	0.7798	2.1

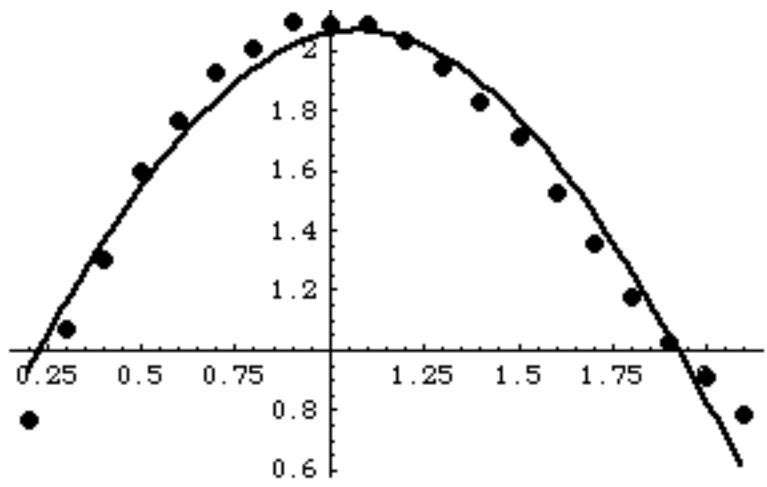


Figure 7: B1 Fitted curve data set 1.
 X-axis: input flip angle, Y-axis: signal intensities Here, $C=1.4479$ radians
 Contains gray and white matter and CSF.

B1 for data set one is calculated to be 0.0673 gauss and the flip angle is 83.00° for this region. This nutation angle is the result of inputting a B1 of 0.146 gauss into the center image plane. This value of B1 has an estimated error value of 0.0181.

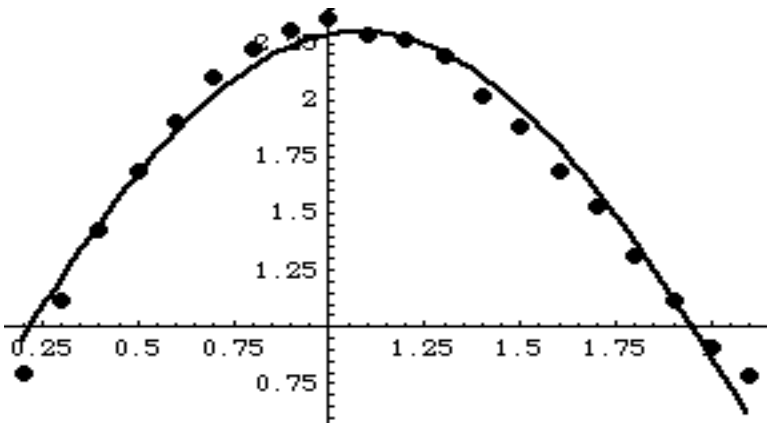


Figure 8: B1 Fitted curve data set 2. X-axis: input flip angle, Y-axis: signal intensities. Here, $C=1.4574$ radians
 Contains gray and white matter and CSF.

B1 for data set two is 0.0677 gauss and the flip angle is 83.54° . The error for this B1 value is 0.0143.

VI. Discussion and Conclusion

T1 Maps

This technique for measuring T1 yielded a low error. Some sources of this error could be credited to variance in several terms. These terms include but may not be limited to B1, the length of the experimental repeat time, or image artifact. For human measurements, motion is also a factor that could contribute to error in this term.

PC Cine Velocimetry

In Figure 5, the graphs seem to vary significantly but actually the mean volume flow rates are similar (Table 3). Still the instantaneous flow rates (Fig. 5 & 6) vary significantly. This is also shown by inspection of the error values, which yielded significantly high values. This variance may be due to limitations in our pulse sequence or changes in the flow characteristics along the phantom. Presently, the instantaneous differences observed here are not explained. This quantity must be further evaluated before a sound conclusion can be reached. It is speculated that the variance in the instantaneous flow measurements could be due to the difference in measurement locations. To address this problem thoroughly, data will be reevaluated once the measurement location of the ultrasound is adjusted to match the observed measurement location of the PC Cine maps. An additional flow probe is being procured for this purpose.

B1 Map

The two B1 map fits show different values for different regions of the specified slice. This is important because it demonstrates that B1 is not a homogeneous quantity. Assuming B1 is homogeneous or miscalculation of this term impacts the accuracy of perfusion measurements: inaccuracy of B1 causes inaccuracy in the calculation of λ which in turn affects the accuracy of λ , the inversion/labeling efficiency. Some sources of error in this term are image artifact and motion. The repeat time (TR), which requires a

value five times that of T_1 , may also be a source of error for B_1 . The estimated error for this term yielded low quantities for both data sets.

Acknowledgements

The author thanks Dr. H. Michael Gach, Weiyang Dai, Prasad Sarma, the MR Research Center at the University of Pittsburgh, the Physics REUFOM at the University of Pittsburgh, and Dr. Kathleen McCloud, Xavier University of Louisiana.

References

- 1-a. J.P. Hornak, "The Basics of MRI", 1996-2002, XII
<http://www.cis.rit.edu/htbooks/mri/inside.htm>
R.V. Damadian
- 1-b European Magnetic Resonance Forum Foundation
"Magnetic Resonance in Medicine — the Basic Textbook of the EMRF Foundation".
1995,2001,2003
<http://www.emrf.org/FAQs%20MRI%20History.html>
2. "Tumor Detection by Nuclear Magnetic Resonance."
Science (March 19, 1971).
3. A. Kumar, D. Welte, R.R. Ernst
"NMR Fourier zeugmatography."
J. Magn. Reson. 18:69-83 (1975)
Naturwissenschaften 62: 34 (1975)
4. How Stuff Works
Todd A. Gould, RT-(R)(MR)(ARRT)
<http://electronics.howstuffworks.com/mri.htm>
5. D. L. Thomas, M. F. Lythgoe, G. S. Pell, F. Calamante, R. J. Ordidge.
The measurement of diffusion and perfusion in biological systems using magnetic resonance imaging. *Phys. Med. Biol.* 45 R97-R138 (2000).
6. Y. Zhang, PhD, H. N. Yueng, PhD, M. O'Donnell, PhD, P.L. Carson, PhD.
Determination of Sample Time for T1 Measurement. *JMRI* 8:675-681 (1998)

7. K. R. Thulborn, F.E. Boada, G. X. Shen, J.D. Christensen, T.G. Reese.
Correction of B1 Inhomogeneities using Echo-Planar Imaging of Water.
MRM 39:369-375 (1998).

8. Electrical and Computer Engineering Department
webmaster@ccem.uiuc.edu
Copyright © 1998-2002
<http://www.ccem.uiuc.edu/resjin1.html>

9. Medical Diagnostic Imaging
Principles and applications for Medical Physics
<http://physics.ramapo.edu/~dbuna/mri.htm>